Springer

KSME

Journal of Mechanical Science and Technology 32 (4) (2018) 1835~1847
www.springerlink.com/content/1738-494x(Print)/1976-3824(Online)
DOI 10.1007/s12206-018-0340-4

The influence of charge air temperature and exhaust gas recirculation on the availability analysis, performance and emission behavior of diesel - bael oil - diethyl ether blend operated diesel engine †

M. Krishnamoorthi* and R. Malayalamurthi

Department of Mechanical Engineering, Government College of Technology, Coimbatore 641013, Tamil Nadu, India

(Manuscript Received July 17, 2017; Revised November 6, 2017; Accepted January 10, 2018)

Abstract

In this work, the first and second laws of thermodynamic analyses were carried out on Kirloskar direct injection, variable compression ratio (VCR) engine at four different charge air temperatures (CAT) and exhaust gas recirculation (EGR) mode. Performance, emission and combustion characteristics along with exergy analysis of ternary test fuel of 60 % diesel + 30 % bael oil + 10 % diethyl ether (DEE) were performed. Various exergy components are identified and calculated individually with the percentage of engine load at 1500 rpm. When operating the diesel engine with 47 °C CAT, brake thermal efficiency (BTE) is improved to 29.33 %, carbon monoxide (CO), hydrocarbon (HC), and emissions have been reduced by 8.57 %, 4.28 % and 6.01 % at peak engine load. The oxides of nitrogen (NOx) have been reduced by 20.12 % at 100 % engine load for 30 % EGR mode. The maximum exergy efficiency of 54.61 % has been observed at full engine load for the 47 °C CAT.

Keywords: Bael oil; Charge air temperature; Diethyl ether; EGR; Exergy

1. Introduction

Direct injection (DI) diesel engines are commonly used for automotive, transportation, industrial and agricultural applications for the reason of their higher fuel conversion, thermal efficiencies and easy operation [1, 2]. The diesel engines are suited for vegetable oils and their esters as they have lower emission level with comparable thermal efficiency [3]. However, the vegetable oils have high viscosity that leads to poor atomization and inefficient combustion [4, 5]. The kinematic viscosity of vegetable oils does not meet the diesel fuel standards prescribed by ASTM, which is 2-3.6 mm^2/sec at 40 °C but the vegetable oils have 10-15 times of fossil diesel viscosity, which can be reduced by the microemulsion process [6]. The vegetable oil viscosity can be reduced by preheating of oil before the injection or by blending with lower viscosity and volatile fuels such as diesel, ethanol, diethyl ether [7, 8]. Thermodynamic first and second laws are applied simultaneously in order to improve the performance, combustion and emission behavior for the internal combustion (CI) engine [9, 10]. In the second law analysis, exergy is a key concept; which is used to indicate the available and unavailable energy [11, 12]. Such analysis is of meticulous significance because this analysis reveals features of the combustion process that cannot be captured by its first law counterpart; such as the detail obtained during the combustion process up to 30 % of fuel availability can be destroyed [13]. Abassi et al. [14] investigated the research work of the CAT effect. They concluded that both the BTE and BSFC decreased slightly with the effect of CAT, which could be attributed to higher heat loss. Contrasting energy, exergy can be destroyed, which is an effect of various phenomena such as combustion, throttling, mixing and etc [15-17].

The useful mechanical work in the IC engines has been improved by reducing the inefficient use of fuel availability that is the destruction of availability [18, 19]. Pan et al. [20] investigated the effect of the CAT. The research work shows that an increase in the inlet air temperature can improve the engine performance and but increase oxides of nitrogen (NOx) and reduce the soot emissions. Kumar et al. [21] investigated the effect of EGR and injection timing on performance and emission behavior of CI engine. They concluded that NOx reduced 12.4 %, opacity lowered 100 % and BSFC increased 2.9 % compared to that of neat diesel in naturally aspirated diesel engine [22]. NOx emissions gradually reduced with EGR rates up to 30 % further increase in EGR drastically increased the smoke opacity. The engine will become anxious along with heavier smoke exposed at the position once the DEE portion

*Corresponding author. Tel.: +91 9940772158, Fax.: +91 4222455230
E-mail address: krishnamoorthism@gmail.com
† Recommended by Associate Editor Jeong Park

increased more than 24 % [23, 24].

Few researchers have conducted experiments with vegetable oil blends in diesel engines. But no one tried the EGR and charge air temperature effects in compression ignition engines with bael oil blends. This investigation analyses the influence of the charge air temperature and exhaust gas recirculation on the availability analysis, performance, emission and combustion characteristics under a steady-state operating condition with ternary test fuel at 1500 rpm engine speed. The exergy examination of CI engine is accompanied by maximizing the work availability and by decreasing the destroyed availability [3, 9].

2. Materials and methods

Aegle marmoles (bael) tree is cultivated all over India, predominantly within sanctuary gardens due to the position as a sanctified tree; likewise northern Malaya and Srilanka [3]. The properties of bael oils are iodine value – 94 mg iodine/g (it belongs to monounsaturated vegetable oil); higher heating value (HHV) – 40040 J/kg; saponification value - 0.205 g/KOH; lower heating value (LHV) – 36300 J/kg [25]. The DEE of 99 % purity purchased from neighborhood business enterprise agent. Bael oil is mixed with diesel and DEE fuel in a blender device and stirred using an electromagnetic agitator at 500 rpm for 20 minutes and left for 30 minutes to accomplish equilibrium with ambient temperature before the experimental trial.

2.1 Fuel properties

First of all, the fuel properties of different fuel blends including kinematic viscosity, and density are determined in line with ASTM D-445 and ASTM D-1298 standards, respectively. The redwood viscometer has been used to determine the kinematic viscosity of liquid fuels [3]. The properties of diesel, bael oil, DEE and its blends are specified in Tables 1 and 2.

2.2 EGR system

The exhaust gases from the exhaust pipe were allowed to enter into the EGR system at 5 meters away from the engine. A piping arrangement of 8 meter length was connected to the exhaust line. The temperatures of the exhaust gases are ensured that their temperatures are approximately equal to the ambient air temperature before the suction manifold without any cooling system [26]. A control valve was fitted with the pipeline, which controls the exhaust gas flow rate and regulates the mixture of exhaust gases with fresh air inducted into the inlet manifold [27]. The fluctuations of the exhaust flow in the exhaust pipe were reduced by the pulse reducer. The K-type thermocouple was used to measure the temperature of charge mixture before the inlet of the engine cylinder [28, 29]. The 'U' tube manometer was used to measure the pressure difference and to obtain the volume of air replaced by exhaust gases on a volumetric basis. The % EGR was calculated using the following equation [26];

% EGR = (volume of air without EGR - volume of air with EGR)/ (volume of air without EGR) ×100.

Table 1. Properties of diesel, bael oil and DEE.

Property	Diesel	Bael oil	DEE
Chemical structure	$C_{16}H_{34}$	$C_{18}H_{36}O_2$	$C_2H_5OC_2H_5$
Density (kg/m^3)	830	896	713
Viscosity (cS)	2.7	24.3	0.23
Auto ignition point (°C)	200-400	< 370	160
Cetane number	50	51.7	> 125
Boiling point (°C)	180-330	298	35
Pour point (°C)	-20	-5	-110
Lower heating value (MJ/kg)	42.8	36.3	33.9
Stoichiometric A/F ratio	14.9	12.4	11.1

Table 2. Properties of fuel blends.

Blend	Kinematic viscosity (cS)	Density in kg/m^{3}at 32 °C	Calorific value (MJ/kg)
60+30+10	8.12	838	40.476

2.3 Charge air temperature (CAT)

The heating of the intake air helps to reduce the engine warm up time, emissions like HC, CO and opacity, and improve the fuel economy [14, 30]. In the air flow circuit, a coil type electric heater is mounted with temperature measuring device and controls the temperature of charge air temperature by the power supply to the heater. For the ideal heating, the air entering the inlet manifold is about 55 °C [22]. The heating of charge air temperature more than 55 °C reduces combustion efficiency and NOx emissions [21, 31]. This is due to the expansion of air during the preheating, diminishing the volumetric efficiency and the oxygen molecules in the inlet charge [20]. From the literature study, the experiments were carried out 27 °C to 57 °C.

2.4 Experimental setup and procedure

The Kirloskar VCR engine has been used for the test and technical specifications are given in Table 3. Fig. 1 shows the schematic diagram of the experimental setup. The charge air temperature is varied by 27 °C, 37 °C, 47 °C, 57 °C and the EGR is varied by 0 %, 10 %, 20 %, 30 % volume fractions [1, 32]. The CAT varied while the EGR maintained at 0 % and EGR rate varied while CAT maintained at 27 °C. Few researchers concluded that the better vegetable oil blends for the compression ignition engines. From the literature survey we took 60 % diesel + 30 % bael oil + 10 % diethyl ether ternary

Table 3. Technical specifications of the test engine.

Type	KIRLOSKAR, VCR multi-fuel, vertical, water cooled, direct injection, naturally aspirated engine
Number of cylinders/ number of strokes	01/04
Rated power	3.5 kW/diesel mode
Bore (mm)/stroke(mm)	87.5/110
Type of ignition	CI
Compression ratio	17.5, varies between 12 to 18
Injection pressure	210 bar
Injection timing	21° bTDC
Speed	1500 Rev/min
Nozzle hole diameter and number	0.3 mm and 3

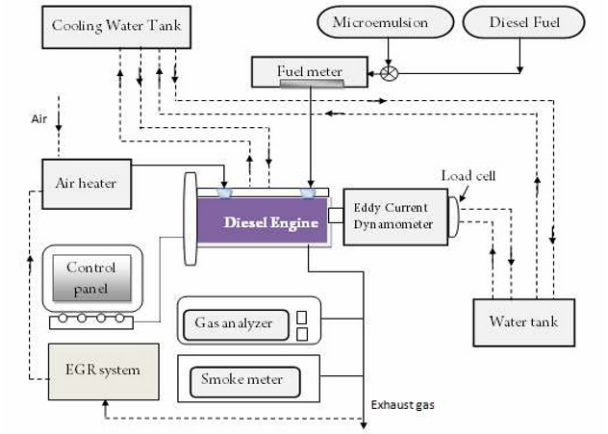

Fig. 1. Schematic diagram.

blend for the experimental work [3-5]. The VCR engine has been operated at different engine loads (0 %, 25 %, 50 %, 75 % and 100 % of maximum engine load) and 1500 rpm [3, 14]. The engine is linked to eddy current dynamometers with proper arrangements in order to provide the load to the engines. CO, CO_2, HC and NOx emissions were calculated by the support of Exhaust gas analyzer AVL DI 444 model (Table 4). Smoke opacity is measured with the support of Smoke meter AVL437C (Table 5). The piezoelectric transducer is located in the cylinder head with the water-cooling system and it is used to measure the cylinder gas pressure. Piezoelectric pressure transducers are appropriate for measuring dynamic and quasi-static, highly dynamic pressure curves or pulsations. The signals from crank angle encoder and charge amplifier are acquired with data acquisition system (DAQ). The apparatus is ideal for test, control, and design applications together with transportable data logging, field monitoring, and in-vehicle data acquisition. The combustion analyses data are usually represented on the basis of degree (°) of crank angle. The crank angle encoder provides an angle and TDC correlation, essential for the calculation of any crank angle based consequence associated with a combustion cycle. The water flow was adjusted to 250 liters per hour for engine cooling according to the information given by engine manufacturer.

3. First law analysis

The fuel incorporates energy on its chemical composition and oxidized with oxygen or air in IC engine. According to the first law, we can calculate the cooling water availability from the coolant inlet and outlet temperature, and the exhaust gas availability from the exhaust gas thermocouple measurements. The IC engine can consider as a control volume (surrounded by control surface) than the energy flows from and to the engine as follows:

The steady flow first law analysis equation [3] for this control volume will be

$$Q_s = P_{shaft} + Q_w + Q_{eg} + Q_{miss}. \quad (1)$$

The terms of Eq. (1) are explained below.

The energy supplied by fuel (Q_s) to the diesel engine given by,

$$Q_s = m_f \times Q_{LHV} \quad (2)$$

where m_f is the mass flow rate of fuel supplied to the engine, Q_{LHV} is the calorific value of the fuel.

The output power delivered (P_{shaft}) by the engine or the shaft power is given by the equation,

$$P_{shaft} = 2 \times \pi \times N(\text{rps}) \times T(\text{N.m}) \quad (3)$$

where $T = (w \times r)$, w is the applied load to the engine by the dynamometer, r is the effective arm radius.

The amount of heat, which is carried away by the cooling water (Q_w) is given by,

$$Q_w = m_w \times C_{pw} \times (T_2 - T_1) \quad (4)$$

where m_w is the mass flow rate (kg/s) of coolant, C_{pw} is the specific heat of coolant, T_2 is the coolant outlet temperature and T_1 is the coolant inlet temperature.

If we know the quantity heat required to increase the temperature of the total mass (m_a and m_g are the mass of air and exhaust gas) with respect to outside atmosphere temperature (T_a) to the exhaust gas temperature (T_g), we can calculate the value of heat loss through the exhaust gases. The average specific heat (C_{pg}) of the exhaust gases are considered as the specific heat of air at mean exhaust temperature [17].

$$Q_{eg} = (m_a + m_g) \times C_{pg} \times (T_g - T_a). \quad (5)$$

In some case, the exhaust gas calorimeter used to measure the thermal energy from the exhaust side. This is an exhaust to water heat exchanger where the exhaust gas is cooled to a moderate temperature (not less than 60 °C, because it is the dew point temperature of exhaust gas) and the energy loss is

calculated by,

$$Q_{eg} = \frac{\dot{m}_c \times C_{pw} \times (T_4 - T_3) \times (T_5 - T_a)}{(T_5 - T_6)} \quad (6)$$

where in m_c is the mass flow rate of water into exhaust gas calorimeter, the calorimeter water inlet temperature is T_3, T_4 is the calorimeter water outlet temperature, the exhaust gas temperature at calorimeter inlet is T_5, T_6 is the exhaust gas temperature at calorimeter outlet and the atmosphere temperature is T_a [13].

The amount of heat transfer to the engine cylinder wall is calculated by [3],

$$\frac{dQ_w}{d\theta} = h_c \times A \times (T_g - T_w) \quad (7)$$

where T_g is the combustion gas temperature, h_c is the convective heat transfer coefficient between the cylinder wall and combustion gas, T_w is the cylinder wall temperature and A is the convection heat transfer area.

Hohenberg's relationship was used for finding the instantaneous heat transfer [3]. The instantaneous heat transfer coefficient across the walls for the engine can be predicted using Eq. (8),

$$h_c = \left(\frac{130 \times p_c^{0.8} \times (v_p + 1.4)^{0.8}}{V^{0.06} \times T_g^{0.4}} \right). \quad (8)$$

The unaccounted losses (Q_{un}) is computed by the energy balance equation and is given by,

$$Q_{un} = Q_s - (P_{shaft} + Q_w + Q_{eg} + Q_{oil}). \quad (9)$$

4. Availability (exergy) analysis

The exergy evaluation referred to diverse forms of control to have different levels of capability toward the positive work output. Availability of a system is defined as the highest work that can be obtained from a system through its reversible process to a state of mechanical, thermal and chemical equilibrium with its environment [12]. In this section, the equations are given, which deals with the exergy balance to the IC engine and its subsystems in order to evaluate the various processes irreversibilities.

Input availability by Ref. [33] used the following relation for,

$$A_{in} = 1.0338 \times Q_{LHV} \quad (10)$$

where 1.0338 is a constant for liquid diesel or blended fuels and varied for gaseous fuels [34];

Shaft availability,

$$\frac{dA_w}{d\theta} = (P_{cyl} - P_a) \times \frac{dV}{d\theta} \quad (11)$$

where $dV/d\theta$ is the rate of change of cylinder volume based on crank angle, P_a indicates the ambient pressure, P_{cyl} is the instantaneous cylinder pressure.

Availability input converted to cooling water availability (A_{cw}),

$$A_{cw} = Q_w - \left[m_w \times C_{pw} \times T_a \times \ln \frac{T_2}{T_1} \right]. \quad (12)$$

Availability transferred to exhaust gases (A_{eg}),

$$A_{eg} = Q_{eg} + \left\{ m_{eg} \times T_a \times C_{pg} \times \ln\left(\frac{T_a}{T_5}\right) - \left(R_{eg} \times \ln\left(\frac{P_a}{P_{eg}}\right)\right)\right\} \quad (13)$$

where R_{eg} is the gas constant for exhaust gas, R_{eg} = R_u/molecular weight, R_u - universal gas constant, Pa is the atmosphere pressure, P_{eg} is the exhaust gas pressure.

The destroyed availability (A_{des}) is determined from the availability balance equation as,

$$A_{des} = A_{in} - (A_{shaft} + A_{cw} + A_{eg}). \quad (14)$$

The ratio of total availability recovered from the system to the total availability input into the system is called exergy efficiency or second law efficiency (η_{II} or δ) [35]. The recovered availability includes A_{shaft}, A_{cw} and A_{eg}.

$$\varepsilon = (\text{availability recovered}) / (\text{availability input})$$
$$\delta = 1 - (A_{des} / A_{in}). \quad (15)$$

5. Results and discussion

In this work the overall performance, combustion, emissions behavior of VCR engine fuelled with ternary blends of bael oil, diesel and DEE were investigated along with an exergy analysis. The behavior of the engine with test modes has been discussed as BTE, BSFC, NOx, CO, CO_2, HC and smoke opacity as a function of the percentage of engine load.

5.1 Availability input

Fig. 2 shows the impact of CAT and EGR on input availability for different engine loads. The air-fuel combinations build up in the combustion chamber to produce higher cylinder gas temperature while increasing the engine load [3]. The input availability has been observed as 702.96 and 878.0 kJ/min for 20 % EGR in 75 % and 100 % engine loads which are 2.77 % and 2.33 % lower than that of 0 % EGR re-

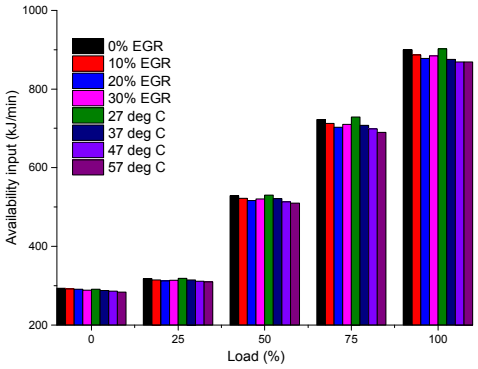

Fig. 2. Availability input.

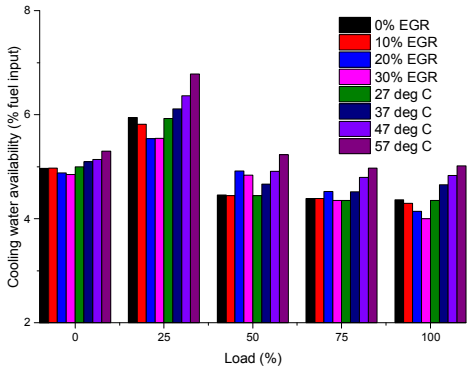

Fig. 3. Cooling water availability.

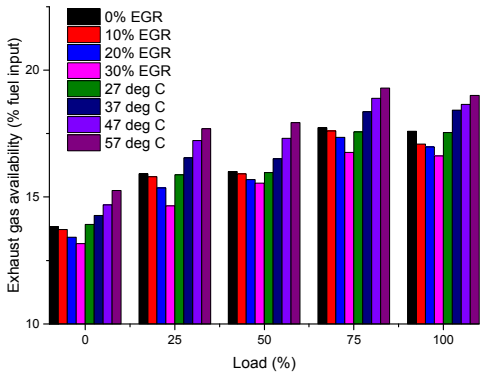

Fig. 4. Exhaust gas availability.

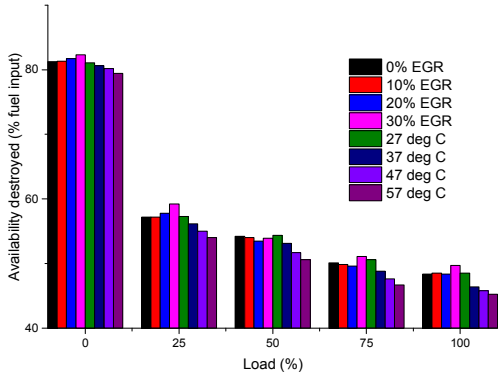

Fig. 5. Destroyed availability.

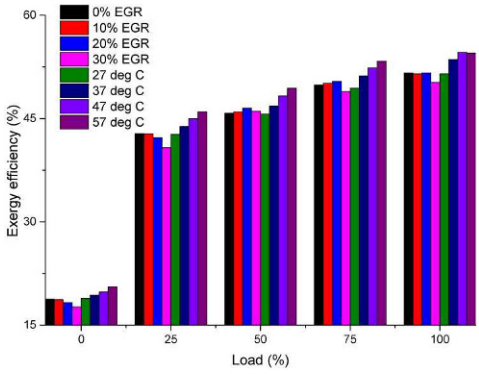

Fig. 6. Exergy efficiency.

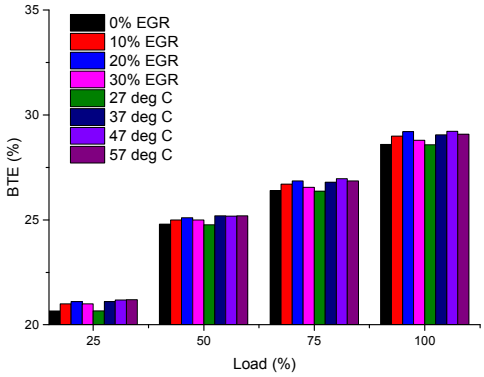

Fig. 7. Brake thermal efficiency.

spectively. For 30 % EGR, the input availability was increased slightly compared to 20 % EGR mode. For EGR, the CO_2 attentiveness in the exhaust gas acts like diluents, which absorbs some quantity of heat and reduces the charge temperature [29]. Therefore for higher EGR condition, more amount of fuel is supplied to produce an equal value of output power [27]. At minimum engine loads, lesser input fuel energy leads to a lesser rate of heat release and therefore reduced cycle temperature and pressure [3]. The preheating of inlet air positively affects the input availability. At 50 % engine load, the input availability has been decreased by escalating the air temperature. The availability inputs were reduced by 2.71 %, 4.12 % and 5.35 % for 37 °C, 47 °C and 57 °C respectively at 75 % engine load which is 728.78 kJ/min for 27 °C. The rising of CAT decreases the quantity of the combustion irreversibilities and reduced the input fuel energy [14]. The increase in CAT leads to higher combustion gas temperature and eventually reduces the combustion irreversibility and also the fuel availability [20].

5.2 Cooling water availability

Fig. 3 indicates the cooling water availability (% of fuel input) for different EGR and CAT as a function of the percent-

age engine load. When increasing the EGR rate, the cylinder gas temperature decreases due to the charge dilution [28]. At 25 % engine load, the cooling water availability to input availability was high compared to medium and peak engine loads. The minimum cooling water availability has been observed for 20 % and 30 % EGR rate as 5.31 and 8.26 % lower compared to 0 % EGR (4.36 % of fuel input) at full engine load. The increasing of EGR fraction decreases the cumulative heat loss exergy [29]. The enhancement of CAT leads to increase in-cylinder gas temperature and thus the combustion process would happen at the peak temperatures, which leads to augmentation in the rate of heat transfer to the cylinder walls and eventually increases the heat loss availability to the fuel availability [14]. Rapid and complete combustion with 57 °C produces maximum combustion temperature and therefore higher exergy transfer to the cylinder walls [29]. From Fig. 3, the cooling water availability (% of fuel input) was higher at 25 % engine loads. This indicates that more fraction of input availability was converted to engine cooling availability loss [3]. At 75 % engine load, the 47 °C and 57 °C CAT conditions the cooling water availability has been observed as 12.6 % and 14.4 % higher compared to 27 °C (27.49 kJ/min). At peak engine load, the cooling water availability has been increased due to progressive combustion, peak cylinder gas temperature and heat transfer [3]. The continuous rise in average cylinder temperature throughout the combustion phase also enhances the contribution of wall heat transfer towards destruction availability [31].

5.3 Exhaust gas availability

The exhaust gas availability for various CAT and EGR has been plotted with the percentage of engine loads as shown in Fig. 4. The temperature of the exhaust gases was lower when the engine is operated with EGR as compared to the operation without EGR [27]. The lowest cooling water availability (% of input availability) was observed throughout the engine operation with 30 % EGR compared to other EGR modes. The escalating rate of EGR reduces the exhaust temperature due to the reduction in availability of O_2 for the combustion and higher specific heat of intake charge mixture [28]. Nevertheless, as overall cycle temperature was decreased with a higher concentration of 30 % EGR, exergy transfer associated with heat transfer was also found to be diminished [29]. The increase in engine load elevates the exhaust gas availability due to more amount of fuel energy supplied for the chemical reaction and produces higher temperature combustion products and leads to exhaust energy loss [3]. An increase in the CAT increases the temperature level in the combustion gases. At 75 % engine load, the exhaust gas availability for 37, 47 and 57 °C have been measured as 18.43, 18.65 and 18.99 % of fuel input respectively which is 158.3 kJ/min for 27 °C. The exhaust gas availability contributes 10-30 % of input availability due to heat transfer along with the combustion products [31].

5.4 Destroyed availability

Fig. 5 shows the destroyed availability (% of fuel input) for different EGR and CAT towards a percentage of engine loads. At no load condition, the destroyed availability was massive due to the zero shaft availability from the engine [3]. The total destroyed availability for 30 % EGR was higher than that of without EGR. The higher destroyed availability was due to lower combustion temperature and more internal heat exchange loss at 57 °C [29]. The rising of combustion temperature decreases the combustion irreversibility, therefore higher cylinder gas temperature at full loads render lesser irreversibility generation [3]. At 75 % and 100 % engine loads, the 30 % EGR has been observed as 50.65 and 49.34 % of availability input respectively which is 50.12 and 48.37 % of availability input (361.97 and 435.37 kJ/min) for 0 % EGR. For the delayed combustion phase, thermo-mechanical availability decreased due to availability destruction caused by work availability and heat transfer, while irreversibility increased due to the irreversibility of burning and incomplete combustion [36]. The quantity of radicals generated during the combustion process and their contents also have a significant consequence on exergy loss [33]. The effect of increasing CAT reduces the destruction availability due to more availability distribution towards the cooling water and exhaust gas availability. At full engine load, the destroyed availability for 37, 47 and 57 °C CAT has been observed as 46.4, 45.78 and 45.21 % of input availability which is 48.51 % of fuel input (437.83 kJ/min). The irreversibility generation with equivalence ratio is majorly attributed to the rise in-cylinder gas temperature and the convective heat transfer coefficient [31]. The availability destruction during the combustions accounts for 40-55 % of the input availability at medium and peak engine loads [3].

5.5 Exergy efficiency

Fig. 6 indicates the exergy efficiency for different operating conditions towards the percentage of engine load. The exergy efficiency was lower for all test modes since the shaft availability becomes zero and most of the availability was shared by the destroyed availability [3]. At 50 % engine load, the exergy efficiency of 20 % EGR has been observed as 46.52 % which is 45.77 % for 0 % EGR. At 75 % and 100 % engine loads, the 30 % EGR has lower exergy efficiency compared to other working conditions. This is due to the addition of EGR lowered the gradient of the thermo-mechanical availability rise due to the decrease in-cylinder gas pressure and temperature [28]. The improvements in combustion results in higher work exergy producing enhanced exergy efficiency. At peak engine load, the minimum exergy efficiency of 50.25 % was found at 30 % EGR due to increased combustion irreversibility and more destroyed availability [29]. An increase in CAT leads to decrease in the entropy generation and increases the exergy efficiency [14]. The growing CAT was positively affecting the exergy efficiency. At peak engine load, the 320 and

57 °C mode have the maximum exergy efficiency of 54.61 and 54.5 % respectively which is 51.48 % for 27 °C. This is due to an efficient increase in combustion gas temperature to bring down the availability destruction in the chemical reaction [31]. From the availability analysis, it emerges to evaluate that preheating the charge or EGR may improve the exergy efficiency.

5.6 Brake thermal efficiency (BTE)

Fig. 7 shows the effect of EGR and CAT on BTE for different engine loads. The successful burning of HC species in the fuel creates to achieve the maximum thermal energy and reduce the fuel consumption [3]. At part engine loads, the use of higher percentages EGR seems to slightly improve the engine performance [26]. At 75 % engine load, the 10 % and 20 % EGR have 26.7 and 26.85 % BTE which is 26.4 % for 0 % EGR. When the engine load increases, the EGR rates are increased that leads to slight increase in the exhaust gas temperature and the entry of intake charge temperature [27]. At full engine load, 20 % EGR has maximum BTE of 29.2 % which is 28.6 % for 0 % EGR. At 30 % EGR, the BTE values reduced due to more amount of fuel burn simultaneously and the combustion is closer to the TDC [29]. The increasing of CAT increases the BTE due to escalating combustion temperature and pressure and reducing consumption of fuel. At 75 % and 100 % engine loads, 47 °C CAT has been observed as 29.05 and 29.23 % of BTE. This is due to the fact that preheating the inlet charge increases the combustion efficiency causing a concurrent rise in-cylinder gas temperature [20]. From Fig. 7, it can be observed that the BTE was decreased with increasing CAT about 57 °C. This is due to the dilution of fuel which leads to increase the BSFC and reduced the burning efficiency [3].

5.7 Brake specific fuel consumption (BSFC)

The BSFC of different EGR and CAT have been plotted towards the percentage of loads as shown in Fig. 8. The BSFC was higher when the engine running at 25 % engine loads. The combustion process was deteriorated at the lower engine loads due to lower in-cylinder temperature [3]. At 25 % engine load, the maximum BSFC was observed for 27 °C CAT as 0.412 kg/kW-hr. The BSFC has decreased while escalating the engine loads due to enhancing cylinder gas pressure and temperature [35]. The lowest BSFC was observed for 20 % EGR at 100 % engine load was 0.283 kg/kW-hr which is 2.4 % lower than that of 0 % EGR. The BSFC for 30 % EGR is slightly higher than 20 % EGR. An additional boost of the EGR beyond critical value results to a more intense increase of the total BSFC [20]. At peak engine loads, thermal efficiency and BSFC are almost similar with EGR compared to without EGR [21]. The total burning rate of fuel is affected by the preheating of inlet air [27]. The growing of CAT reduces the chance of condensation of fuel in the combustion chamber

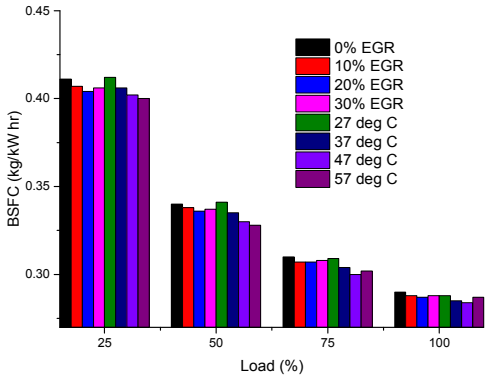

Fig. 8. Brake specific fuel consumption.

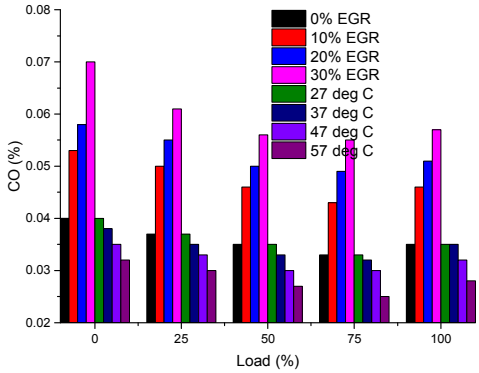

Fig. 9. Carbon monoxide.

[20]. At 75 % and 100 % engine loads, the BSFC for 47 °C CAT has been observed as 0.3 and 0.28 kg/kW-hr which is 0.313 and 0.291 kg/kW-hr for 27 °C CAT. The BSFC for 57 °C mode was slightly improved at higher engine loads due to the effect of charge dilution at peak combustion temperature [3].

5.8 Carbon monoxide emissions (CO)

Fig. 9 shows the influence of blended fuel on CO emissions for various values of EGR and CAT. Injection pressure, air-fuel fraction, engine load, fuel type and intake charge temperature influence the CO emissions [3]. An incomplete combustion of fuel and inadequate mixing of fuel/air leads to incomplete combustion [37]. At lower engine loads, the long ignition delay and slow burning of fuel weaken the combustion process and increases CO emissions [38]. For EGR condition, the minimum CO emissions were observed at 75 % engine loads. The 0 % EGR has minimum CO emission of 0.035 % at 75 % engine load which is 0.057 % for 30 % EGR. For 100 % engine load with EGR condition, CO emission was increased slightly compared to 75 % engine loads. The preheating of intake air up to elevated temperature subsequently reduces CO emission. This is due to the fact that better evaporation and shorter ignition delay engine will produce low noise and vibration [30]. The lowest CO emission observed for

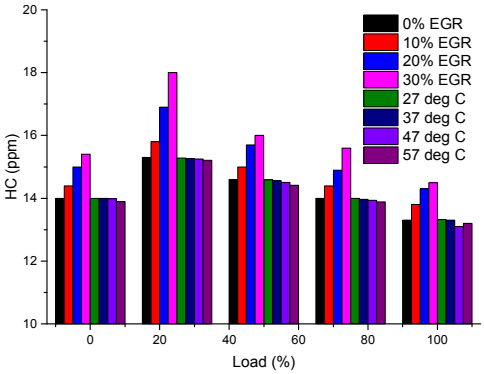

Fig. 10. Hydrocarbon.

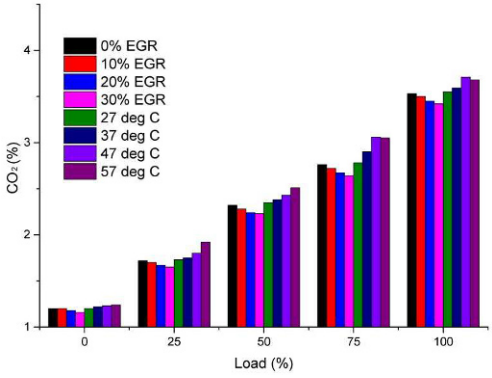

Fig. 11. Carbon dioxide.

57 °C at 75 % engine load was 0.025 % which is 0.033 % for 27 °C CAT. The reason is that the CAT is an important factor for creating the homogeneous mixture [20]. At full engine load, CO emission for 57 °C CAT has been observed as 0.028 % which is 0.035 % for 27 °C CAT. The dilution effect of CO_2 contributed to incomplete combustion and consequently results in higher CO emission [29].

5.9 Hydrocarbon emissions (HC)

Fig. 10 shows the effect of EGR and CAT on HC emissions for different engine loads. HC emissions diminish with a rise in engine loads because of enhancement of combustion process [3]. At 25 % engine load, the maximum HC has been observed as 18 ppm for 30 % EGR which is 15.3 ppm for 0 % EGR. The lesser oxygen concentration with EGR system results in rich air-fuel mixtures at various locations within the combustion chamber. At elevated engine loads, HC emission is reduced, because at the elevated temperature the HC species can be burned easily [3]. For EGR, the least HC emission was observed as 14 ppm for 0 % EGR at 100 % engine load. At maximum engine load with EGR mode, CO emission is slightly reduced. This is because of the large amount of fuel injected at full loads burns rapidly and hence rapid heat release increases peak temperature [29]. The effect of CAT decreases the HC emissions with escalating the percentage of engine loads. Minimum HC emission observed at full engine load was 13.1 ppm for 47 °C CAT which is 13.32 ppm for 27 °C CAT. HC emission for 57 °C CAT was slightly increased compared to 47 °C CAT at full engine load. The vaporized fuel from sac volume and nozzle holes are mixed with air in the expansion stroke and this part of the fuel remains unburned and leads to HC emission [3].

5.10 Carbon dioxide emissions (CO_2)

Fig. 11 shows the influence of EGR and CAT on CO_2 emission towards the percentage of engine loads. The CO_2 and water vapor are assumed to be end products of HC fuel when completely oxidized [3]. At lower engine loads, CO_2 emission

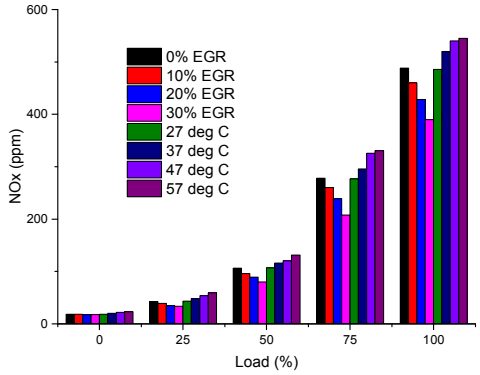

Fig. 12. Oxides of nitrogen.

was lower due to the inefficient burning of fuel at lower combustion temperature [37]. At 25 % engine load, 0 % EGR has peak CO_2 value of 1.72 % which is 1.65 % for 30 % EGR. At peak engine load, 0 % EGR has 3.53 % of CO_2 emission which is 3.11 % higher compared 30 % EGR mode. The complete burning of fossil fuels has been directly indicated by CO_2 emission exhaust [3]. The rising of CAT enhances the CO_2 emission which leads to complete combustion. At 75 % and 100 % engine loads, CO_2 emission for 47 °C CAT has been observed as 3.06 % and 3.71 % which is 9.15 % and 4.31 % higher than 27 °C CAT mode. More CO_2 will reduce the specific heat of the air-fuel mixture and thus, the cylinder pressure and temperature are decreased at the end of compression stroke [26]. For 57 °C CAT operation has slightly lower CO_2 emissions due to inefficient burning and charge dilution which leads to reduction in the combustion efficiency [3].

5.11 Nitrogen oxides emissions (NOx)

Fig. 12 indicates the effect of EGR and CAT on NOx emission for different engine loads. The NOx emission decreases with the increasing EGR rates [29]. The EGR in diesel engines has reduced the oxygen molecules in the fresh air and reduced the flame temperature in the combustion gases [39]. At half engine load, minimum NOx has been observed for 30 % EGR was 208 ppm which is 25.1 % lesser compared to

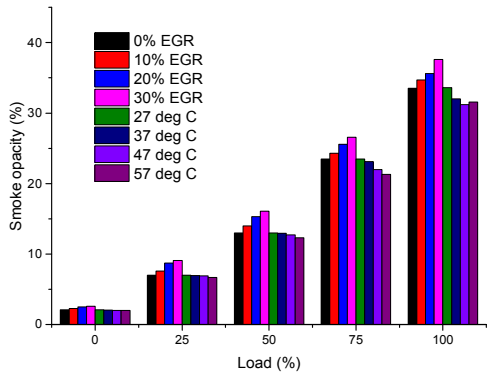

Fig. 13. Smoke opacity.

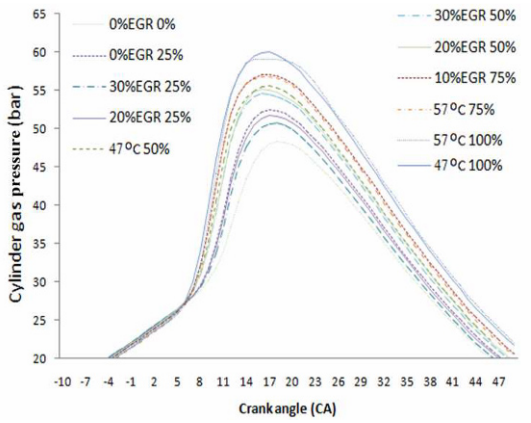

Fig. 14. Cylinder gas pressure.

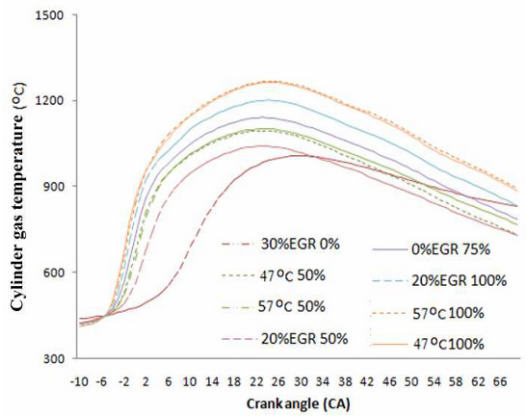

Fig. 15. Cylinder gas temperature.

0 % EGR. At 50 % engine load, oxygen has been present in satisfactory amount but at 100 % loads, oxygen reduces significantly which leads to reduced NOx emissions at the peak engine loads [40]. At full engine load, 30 % EGR has 20.12 % lower NOx emission which is 488 ppm for 0 % EGR mode. As the in-cylinder temperature drops ultimately if supplied more level of EGR rate about 60 % [26]. This is due to the air flow rate decreased and fuel flow rate increased with increase in CAT, which enhances the combustion temperature [31]. At 75 % engine load, highest NOx emission has been observed for 57 °C CAT as 331 ppm which is 277 ppm for 27 °C CAT mode. At full engine load, the NOx emissions for 47 °C CAT mode was 540.5 ppm which is 0.935 % lower than 57 °C CAT mode. This is primarily attributed towards the lower combustion temperature and delay in initiation of combustion, particularly during the early stage of the combustion phase [27].

5.12 Smoke opacity

Fig. 13 shows the percentage of smoke opacity for various EGR and CAT towards engine loads. The increase of EGR rate results in an increase of soot concentration i.e. at minimum load it is up to 20 % while at maximum load the soot increases up to 40 % [27]. At half engine load, smoke for 30 % EGR has been measured as 16.1 % which is 19.25 % higher than 0 % EGR mode. The reason for lowest smoke opacity was owing to the lack of rich fuel pockets inside the combustion chamber [20]. At full engine load, 20 % EGR has 3.75 % lesser smoke value compared to 30 % EGR mode (37.6 %). The smoke oxidation also depends on the air temperature [22]. The higher CAT the elevated temperature on the flame front burns more soot [30]. At 75 % engine load, least amount smoke opacity has been observed for 57 °C CAT was 21.3 % which is 23.5 % for 27 °C CAT mode. At peak engine load, the least smoke opacity has been observed for 47 °C CAT mode as 31.2 % which is 7.14 % lower compared to 27 °C CAT mode. This is probably due to the higher cylinder gas temperature restricting the soot formation and also initiating the combustion at earlier [27].

5.13 Maximum cylinder gas pressure

Fig. 14 shows the cylinder gas pressure variation against crank angle (-10° to 50° reference toward TDC). The rate of pressure rise depends on the combustion of fuel in the duration of premixed combustion phase is the base for CI engine [3]. The combustion curves were developed by averaging of ten test cycle. As the EGR rate increases, the ignition delay of the mixture increase and retards the combustion phase correspondingly as well as the peak pressure decreased [28]. By rising CAT, the rate of cylinder pressure becomes higher during the initial stage of combustion and the peak pressure occurs slightly earlier compared to without EGR condition [41]. The increased EGR rate leads to delay in auto-ignition, therefore the main combustion stage moves towards the expansion stroke [26]. Maximum cylinder gas pressure in CI engines depends on the combustion in premixed stage [3]. This short combustion phase further depends on fuel type, mixing of air and fuel, equivalence ratio and engine load [29].

5.14 Maximum cylinder gas temperature

Fig. 15 indicates the average maximum cylinder gas tem-

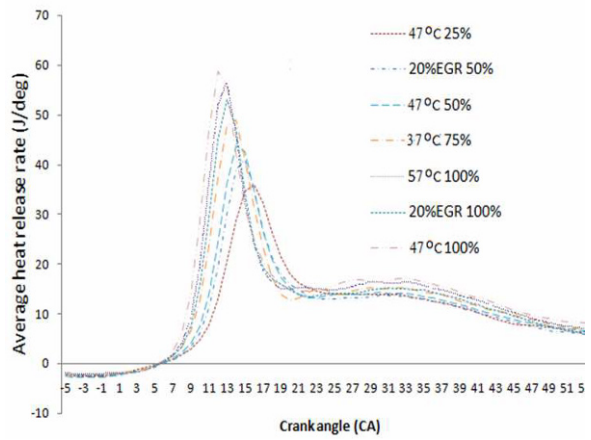

Fig. 16. Heat release rate.

perature with respect to the crank angle (-10° to 70° reference toward TDC). This is the fact that increasing the EGR % will lower down in-cylinder temperature near the end of the compression stroke and cool down the in-cylinder atmosphere [28]. This is the result for both higher premixed controlled combustion and earlier initiation of combustion of the liquid fuel, which occurs due to the higher CAT [30]. The increasing of CO_2 molecules reduces the oxidizing ability of CO which results in reducing of cylinder gas pressure and temperature [28]. The reduction of peak combustion gas temperature leads to decrease in NOx emission [3]. In lower CAT operation, the fuel burning rates are higher due to long ignition delay and results that higher the cylinder gas temperature rise [30]. For 30 % EGR, the combustion occurs with no strength due to incomplete combustion, lower flame propagation and longer combustion period [28].

5.15 Average heat release rate (HRR)

Fig. 16 shows the average heat release rate (HRR) as a function of crank angle (-20 and 40° reference to TDC). The lower availability of oxygen molecules lowers the intensity of the combustion which lengthens the duration of combustion [28].

The increasing EGR rate decreases HRR owing to incomplete combustion [27]. The combustion rate in the first stage of combustion increases slightly with the increase in CAT. This is due to the more quantity of fuel burned during the first combustion phase and also the combustion of the vaporized fuel not yet progressed in the combustion chamber with the existing flame front [3]. The rate of ignition delay rise with CAT become more evident for higher engine loads compared to lower engine loads [21]. By escalating the CAT of 20 °C led that the HRR has advanced 4 crank angle degrees (CAD) and the cylinder gas pressure has advanced 3 CAD [36]. From Fig. 16, a decrease in combustion duration with CAT modes shows that combustion finishes much quicker for 57 °C compared to 27 °C mode [29].

Table 4. Technical specifications of gas analyzer AVL DI444.

Measured quantity	Measuring range	Accuracy
Carbon monoxide (CO)	0-10 % vol	< 0.6 % vol: ± 0.03 % vol ≥ 0.6 % vol : ± 5 % vol
Hydrocarbon (HC)	0-20000 ppm vol	< 200 ppm vol : ± 10 ppm vol ≥ 200 ppm vol : 5 %
Oxides of nitrogen (NOx)	0-5000 ppm vol	< 500 ppm vol : ± 50 ppm vol ≥ 500 ppm vol : ± 10
Carbon dioxide (CO_2)	0-20 % vol	< 10 % vol : ± 0.5 % vol ≥ 10 % vol : ± 5 % vol

Table 5. Technical specifications of smoke meter AVL 437C.

	Opacity	Rpm
Measuring range	0-100 %	400-6000
Accuracy & repeatability	±1 % of full scale	±10
Resolution	0.1 %	±1

Table 6. Uncertainties of some measured and calculated parameters.

S. No	Parameter	Percentage uncertainties
1	NOx	±0.1
2	CO	±0.01
3	CO_2	±0.3
4	HC	±0.1
5	Smoke opacity	±0.5
6	BSEC	±1.5
7	BTE	±1
8	Stopwatch	0.01 sec
9	Speed indicator	5 rpm
10	Graduated burette scale	0.001 m
11	Load cell (strain gauge)	0.1 kg

6. Uncertainty analysis

Uncertainties and errors in the experimental analysis may occur due to instruments selection, calibration, working condition, observation, environment and method of the tests [42, 3]. The terms error and uncertainty are often used interchangeably to describe both imperfection and inaccuracy. The instruments for measurements are chosen with a view to keeping the experimental uncertainties as minimum as possible. The uncertainties have been calculated by Eq. (16);

$$\frac{\Delta q}{q}=\sqrt{\left[\frac{\Delta x}{x}\right]^2+....+\left[\frac{\Delta z}{z}\right]^2+\left[\frac{\Delta u}{u}\right]^2+...+\left[\frac{\Delta w}{w}\right]^2}\ . \qquad (16)$$

The uncertainty examination is essential to confirm the precision of the experiments. Uncertainties of few calculated and measured parameters are given in Table 6. Based on the above value, the calculated engine performance is believed to be accurate within ±3 % [3].

7. Conclusion

The important conclusions drawn from the present study include the following. From the exergy analysis, the increasing of CAT causes increased cooling water availability, exhaust gas availability, exergy efficiency and reduced the input availability.

- At peak engine load, the input availability for 37 °C and 47 °C have been observed as 875.1 kJ/min and 868.9 kJ/min which is 902.43 kJ/min for 27 °C CAT.
- The minimum cooling water availability has been observed for 20 % and 30 % EGR rate is 5.31 and 8.26 % lower compared to no EGR (4.36 % of fuel input) at full engine load. The exhaust gas availability contributes 10-30 % of input availability due to heat transfer along with the combustion products.
- At full engine load, the 30 % EGR rate has been observed in 49.34 % of availability input which is 48.37 % of availability input for 0 % EGR mode.
- The minimum exergy efficiency of 51.26 % was found at 30 % EGR with full engine load due to increased combustion irreversibility and more destroyed availability. At full engine load, the 47 and 57 °C CAT have the maximum exergy efficiency of 54.61 % and 54.5 % which is 51.48 % for 27 °C CAT.
- At peak engine load, 20 % EGR had 2.09 % more BTE compared to that of no EGR. The BTE was decreased with increasing of CAT about 57 °C. The 2.4 % lesser BSFC was observed for 20 % EGR compared to that of 0 % EGR at full engine load.
- The preheating of intake air subsequently reduces CO emission. The minimum CO emission was observed for 57 °C CAT at 75 % engine load as 0.025 % which is 0.033 % for 27 °C CAT. For EGR, the minimum HC emission was observed as 14 ppm for 0 % EGR at full engine load. HC emission was observed 1.7 % lower for 47 °C CAT compared to that of 27 °C CAT.
- At full engine load, the NOx emissions for 47 °C CAT mode has 540.4 ppm which is 0.935 % lower than that of 57 °C CAT. At peak engine load, the minimum smoke opacity has been observed for 47 °C CAT mode as 31.2 % which is 7.14 % lower compared to 27 °C CAT mode.

According to the above consequences, it is probable to achieve a good balance between the availability terms, which leads to the improved engine design.

Nomenclature

ASTM : American society for testing and materials
BSFC : Brake specific fuel consumption (kg/kW hr)
BTE : Brake thermal efficiency (%)
CA : Crank angle (deg)
CAT : Charge air temperature (°C)
CE : Chemical energy (J)
CI : Compression ignition
CN : Cetane number
CO : Carbon monoxide (%)
CO_2 : Carbon dioxide (%)
CR : Compression ratio
D : Neat diesel
DEE : Diethyl ether
EGR : Exhaust gas recirculation (%)
HC : Hydrocarbon (ppm)
HRR : Heat release rate (J/deg CA)
IC : Internal combustion
LHV : Lower heating value (kJ/kg)
NOx : Oxides of nitrogen (ppm)
Q_s : Heat supplied (kJ/min)
P_{shaft} : Useful shaft power (kJ/min)
Q_w : Heat transfer through cooling water (kJ/min)
Q_{eg} : Heat transfer through exhaust gas (kJ/min)
Q_{miss} : Miscellaneous heat transfer (kJ/min)
T_a : Ambient temperature (K)
P_a : Ambient pressure (bar)
γ : Ratio of specific heats
η II or δ : Exergy efficiency
θ : Crank angle (deg)
ρ : Density (kg/m^3)
υ : Viscosity (centistokes)

Subscripts

a : Atmosphere condition
cw : Cooling water
des : Destroyed
eg : Exhaust gas
in : Input

References

[1] V. T. Chau, K. P. Charoenphonphanich, S. Sato and H. Kosaka, Optical study on combustion characteristics of hydrotreated vegetable oil and blends under simulated CI engine conditions and various EGR, *Journal of Mechanical Science and Technology*, 31 (9) (2017) 4521-4531.

[2] V. P. Singh and S. R. Chauhan, Feasibility of a new non-edible feedstock in diesel engine: Investigation of performance, emission and combustion characteristics, *Journal of Mechanical Science and Technology*, 31 (4) (2017) 1979-1986.

[3] M. Krishnamoorthi and R. Malayalamurthi, Experimental investigation on performance, emission behavior and exergy analysis of a variable compression ratio engine fueled with diesel- aegle-marmoles oil-diethyl ether blends, *Energy*, 128 (2017) 312-328.

[4] P. M. Shameer and K. Ramesh, Green technology and performance consequences of an eco-friently substance on a 4-stroke diesel engine at standard injection timing and com-

pression ratio, *Journal of Mechanical Science and Technology*, 31 (3) (2017) 1497-1507.

[5] M. Krishnamoorthi and R. Malayalamurthi, Combined effect of compression ratio, injection pressure and injection timing on performance and emission of a DI compression ignition engine fueled with diesel- aegle marmelos oil-diethyl ether blends using response surface methodology, *Energy and Fuel*, 31 (2017) 11362-11378.

[6] P. Emberger, D. Hebecker, P. Pickle, E. Remmele and K. Thuneke, Emission behaviour of vegetable oil fuel compatible tractors fuelled with different pure vegetable oils, *Fuel*, 167 (2016) 288-294.

[7] R. Sakthivel, K. Ramesh, R. Purnachandran and P. M. Shameer, A review on the properties, performance and emission aspects of the third generation biodiesels, *Renewable and Sustainable Energy Reviewers*, 82 (3) (2018) 2970-2992.

[8] H. Xu, B. Yin, S. Liu and H. Jia, Performance optimization of diesel engine fueled with diesel-jatropha curcas biodiesel blendd using response surface methodology, *Journal of Mechanical Science and Technology*, 31 (8) (2017) 4051-4059.

[9] Y. Azoumah, J. Blin and T. Daho, Exergy efficiency applied for the performance optimization of a direct injection compression ignition engine using biofuels, *Renewable Energy*, 34 (2009) 1494-1500.

[10] Y. Li, M. Jia, Y. Chang, S. L. Kokjohn and R. D. Reitz, Thermodynamic energy an exergy analysis of three different engine combustion regimes, *Applied Energy*, 180 (2016) 849-858.

[11] C. D. Rakopoulos and E. G. Giakoumis, Second law analysis applied to internal combustion engines operation, *Progress Energy and Combustion Science*, 32 (2006) 2-47.

[12] C. D. Rakopoulos, M. A. Scott, D. C. Kyritsis and E. G. Giakoumis, Availability analysis of hydrogen/natural gas blends combustion in internal combustion engine, *Energy*, 33 (2008) 248-255.

[13] P. R. Kumaar, M. K. Mishra, S. K. Singh and A. Kumar, Experimental evaluation of waste plastic oil and its blends on a single cylinder diesel engine, *Journal of Mechanical Science and Technology*, 30 (10) (2016) 4781-4789.

[14] A. Abassi, S. Khalilarya and Jafarmadar, The influence of the inlet charge temperature on the second law balance under the various operating engine speed in a DI diesel engine, *Fuel,* 89 (9) (2010) 2425-2432.

[15] S. Jafarmadar, Exergy analysis of hydrogen/diesel combustion in a dual fuel engine using three-dimensional model, *Hydrogen Energy*, 39 (2014) 9505-9514.

[16] A. Abusoglu and M. Kanolu, First and second law analysis of diesel engine powered cogeneration systems, *Energy Conversion Management*, 49 (2008) 2026-2031.

[17] M. J. Abedan, H. H. Masjuki, M. A. Kalam, A. Sanjid, S. M. Ashrafur Rahman and B. M. Masum, Energy balance of internal combustion engines using alternative fuels, *Renewable and Sustainable Energy Reviewers*, 26 (2013) 20-33.

[18] E. G. Giakoumis, Cylinder wall insulation effects on the first and second law balances of a turbocharged diesel engine operating under transient load conditions, *Energy Conversion Management*, 48 (2007) 2925-2933.

[19] M. Krishnamoorthi and R. Malayalamurthi, Availability analysis, performance, combustion and emission behavior of bael oil-diesel-diethyl ether in a variable compression ratio diesel engine, *Renewable Energy*, 119 (2018) 235-252.

[20] W. Pan, C. Yao, G. Han, H. Wel and Q. Wang, The impact of intake air temperature on performance and exhaust emissions of a diesel methanol duel fuel engine, *Fuel*, 162 (2015) 101-110.

[21] B. R. Kumar and S. Saravanan, Effect of exhaust gas recirculation on performance and emissions of a constant speed DI diesel engine fueled with pentanol/diesel blends, *Fuel*, 160 (2015) 217-226.

[22] H. Lee, T. Ha and Hoimyung, Experimental verification of optimized NOx reduction strategies in a decrepit Euro-3 diesel engine retrofitted with a cooled EGR system, *Journal of Mechanical Science and Technology*, 30 (6) (2016) 2873-2880.

[23] M. Karabektas, G. Ergen and M. Hosoz, The effects of using diethyl ether as additive on the performance and emission of a diesel engine fuelled with CNG, *Fuel*, 115 (2014) 885-860.

[24] H. Venu and V. Madhavan, Influence of diethyl ether addition in ethanol-biodiesel-diesel (EBD) and methanol-biodiesel-diesel (MBD) blends in a diesel engine, *Fuel*, 189 (2017) 377-390.

[25] S. K. Katagi, S. R. Munnolli and M. K. Hosamani, Unique occurrence of unusual fatty acid in the seed oil of aegle marmoles corre: screening the rich source of seed oil for bioenergy production, *Applied Energy*, 88 (5) (2011) 1797-1802.

[26] X. Shan, Y. Qian, L. Zhu and X. Lu, Effects of EGR rate and hydrogen/carbon monoxide ratio on combustion and emission characteristics of biogas/diesel dual fuel combustion engine, *Fuel*, 181 (2016) 1050-1057.

[27] P. G. Papagiannakis, Study of air preheated and EGR impacts for improving the operation of compression ignition engine running under dual fuel mode, *Energy Conversion Management*, 68 (2013) 40-53.

[28] S. Jafarmadar and P. Nemati, Analysis of exhaust gas recirculation (EGR) effects on exergy terms in an engine operating with diesel oil and hydrogen, *Energy*, 126 (2017) 746-755.

[29] S. Verma, L. M. Das and S. C. Kaushik, Effects of varying composition of biogas on performance and emission characteristics of compression ignition engine using exergy analysis, *Energy Conversion Management*, 138 (2017) 346-359.

[30] P. Nemeti, S. Jafarmadar and H. Taghavifar, Exergy analysis of biodiesel combustion in a direct injection compression ignition engine using quasi- dimensional multi-zone model, *Energy*, 115 (2016) 528-538.

[31] S. Ismail and S. P. Mehta, Second law analysis of hydrogen-air combustion in a spark ignition engine, *Hydrogen Energy*, 36 (1) (2011) 931-946.

[32] J. I. J. R. Lalvani, M. Parthasarathy, B. Dhinesh and K.

Annamalai, Experimental investigation of combustion, performance and emission characteristics of a modified piston, *Journal of Mechanical Science and Technology*, 29 (10) (2015) 4519-4525.

[33] V. Chintala and K. A. Subramanian, Assessment of maximum available work of a hydrogen fueled compression ignition engine using exergy analysis, *Energy*, 67 (2014) 162-175.

[34] B. B. Sahoo, K. U. Saha and N. Sahoo, Theoretical performance limits of a syngas-diesel fueled compression ignition engine from second law analysis, *Energy*, 36 (2) (2011) 760-769.

[35] N. R. Palani and K. Pitchandi, Spray characterristics of diesel and derivates in direct injection diesel engines with varying injection pressures, *Journal of Mechanical Science and Technology*, 29 (10) (2015) 4465-4471.

[36] H. Feng, C. H. Zhang, M. Wang, D. Liu, X. Yang and L. Chiafon, Availability analysis of n-heptane/iso-octane blends during low-temperature engine combustion using a single-zone combustion model, *Energy Conversion Management,* 84 (2014) 613-622.

[37] M. Razmara, M. Bidarvatan, M. Shahbakhti and R. D. Robintt Ill, Optimal exergy-based control of internal combustion engines, *Applied Energy*, 183 (2016) 1389-1403.

[38] K. Muralidharan and D. Vasudevan, Performance, emission and combustion characteristics of a variable compression ratio engine using methyl esters of waste cooking oil and diesel blends, *Applied Energy*, 88 (11) (2011) 3959-3968.

[39] P. M. Shameer and K. Ramesh, Experimental evaluation on performance, combustion and influence of in-cylinder temperature on NOx emission in a DI diesel engine using thermal imager for various alternative fuel blends, *Energy*, 118 (2017) 1334-1344.

[40] S. Jindal, B. P. Nandwana, N. S. Rathore and V. Vashistha, Experimental investigation of the effect of compression ratio and injection pressure in a direct injection diesel engine running on jatropha methyl ester, *Applied Thermal Engineering*, 30 (5) (2010) 442-448.

[41] S. H. Yoon and S. H. Park, Experimental investigation on the influence of engine operating conditions on combustion and nanoparticle emission characteristics of a small DI diesel engine, *Journal of Mechanical Science and Technology*, 30 (6) (2016) 2839-2848.

[42] J. B. Heywood, *Internal combustion engine fundamentals*, New York USA, McGraw-Hill (1988).

M. Krishnamoorthi received the Master of Engineering (Thermal Engineering) degree from Anna University, Chennai, India. Presently he is pursuing his Ph.D. from Anna University, Chennai, India. His main research areas are thermodynamics, IC engines and alternative fuels.

R. Malayalamurthi, born in 1965, is Associate Professor in the Department of Mechanical Engineering, Government College of Technology, Coimbatore, Tamil Nadu, India. He received his doctoral degree from Anna University of Chennai, India in 2008. He published 30 research articles in international journals.